

REPORT DOCUMENTATION PAGE

Form Approved
OMB No. 0704-0188

The public reporting burden for this collection of information is estimated to average 1 hour per response, including the time for reviewing instructions, searching existing data sources, gathering and maintaining the data needed, and completing and reviewing the collection of information. Send comments regarding this burden estimate or any other aspect of this collection of information, including suggestions for reducing the burden, to the Department of Defense, Executive Service Directorate (0704-0188). Respondents should be aware that notwithstanding any other provision of law, no person shall be subject to any penalty for failing to comply with a collection of information if it does not display a currently valid OMB control number.

PLEASE DO NOT RETURN YOUR FORM TO THE ABOVE ORGANIZATION.

1. REPORT DATE (DD-MM-YYYY) 31-12-2009		2. REPORT TYPE Final Report		3. DATES COVERED (From - To) From 30-08-2006 To 31-12-2009	
4. TITLE AND SUBTITLE Novel Nano-particle, Temperature-Independent Damping System: Basic Science and Applications				5a. CONTRACT NUMBER FA9550-05-1-0185	
				5b. GRANT NUMBER	
				5c. PROGRAM ELEMENT NUMBER	
				5d. PROJECT NUMBER	
				5e. TASK NUMBER	
				5f. WORK UNIT NUMBER	
6. AUTHOR(S) Keer, Leon M.					
7. PERFORMING ORGANIZATION NAME(S) AND ADDRESS(ES) Northwestern University				8. PERFORMING ORGANIZATION REPORT NUMBER	
9. SPONSORING/MONITORING AGENCY NAME(S) AND ADDRESS(ES) Air Force Office of Scientific Research 875 N Randolph St, Ste 325 Arlington, VA 22203				10. SPONSOR/MONITOR'S ACRONYM(S) AFOSR	
				11. SPONSOR/MONITOR'S REPORT NUMBER AFRL-OSR-VA-TR-2013-0915	
12. DISTRIBUTION/AVAILABILITY STATEMENT Distribution A: Approved for public release					
13. SUPPLEMENTARY NOTES Prepared in cooperation with Professors Randall Q. Snurr and Q. Jane Wang and with Dr. Binoy Shah.					
14. ABSTRACT This project envisions a novel concept of mechanical damping: using nanoparticles or microparticles as a damping medium and the interfacial forces as the absorbing mechanism. For thrust damping or radial damping, the mechanical components of the dampers are filled with selected particles. The advantages of particle damping over the conventional damping mechanism are as follows: 1. The performance of the small particles will be temperature independent and therefore the damping device can work in all temperature ranges. 2. The particle size is much smaller than the scale of the container surface roughness, therefore the particles will fill the asperities and create an "ideally smooth" mating surface allowing uniform transmission of shock force from one surface to another. 3. Since the absorbing function is provided by particle reassembly, fatigue is not expected to occur.					
15. SUBJECT TERMS nanoparticles, microparticles, particle-based damping, thrust damping, box damping					
16. SECURITY CLASSIFICATION OF:			17. LIMITATION OF ABSTRACT	18. NUMBER OF PAGES	19a. NAME OF RESPONSIBLE PERSON
a. REPORT	b. ABSTRACT	c. THIS PAGE			19b. TELEPHONE NUMBER (Include area code)

December 31, 2009

**Novel Nano-particle, Temperature-Independent Damping System:
Basic Science and Applications**

Final Report

Principle Investigator: Leon M. Keer

Northwestern University
A319 Technological Institute
2145 Sheridan Road
Evanston, IL 60208-3109

Agreement Number: FA9550-05-1-0185
Program Manager: Dr. Victor Giurgiutiu

20130918432

Objectives

Introduction

Mechanical damping devices are widely used in aircraft and aerospace applications for shock, vibration and force absorption. Reliable dampers are the first protection of mechanical systems against impact and other types of damage. However damper reliability is always an issue for mechanical systems and is becoming a more serious concern for developing future long-range, long-life air force and aerospace systems. Currently, most damping devices use hydraulic or mechanical damping mechanisms. The performance of current hydraulic working fluid is strongly temperature dependent, which makes the reliability of current damping components uncertain in a single mission under the changing location of a system from the Equator to the Arctic Circle. On the other hand, mechanical absorbers possess uncertain reliability when subjected to serious cyclic loading and, therefore, to life threatening fatigue.

Concept of a Particle Damper

This project conceives a novel concept of mechanical damping: using nanoparticles as a damping medium and the interfacial forces as the absorbing mechanism. For thrust damping or radial damping, the mechanical components of the dampers are filled with properly selected nanoparticles.

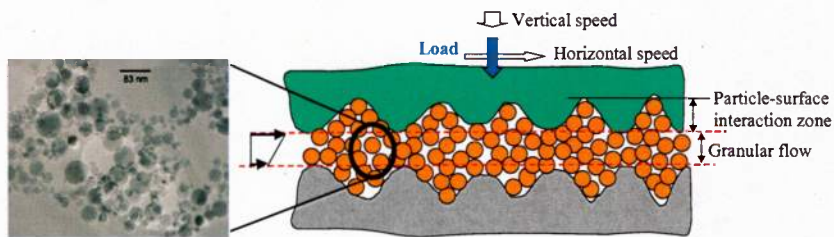


Figure1: Alumina nanoparticles (left), Granular flow regime between asperities(right)

The advantages of particle damping over the conventional damping mechanism are as follows:

1. The performance of the nanoparticles will be temperature independent and therefore the damping device can work in all temperature ranges.
2. The particle size is much smaller than the scale of the container surface roughness, therefore the particles will fill the asperities and create an "ideally smooth" mating surface allowing uniform transmission of shock force from one surface to another.
3. Since the absorbing function is provided by particle reassembly, fatigue is not expected to occur.

Status of Effort

In the previous year (2007-2008), we reported the development of a magnetic particle-based damper using millimeter-size metallic particles as the damping medium in our experiment. Second, we used particle dynamics simulations to model the transient vibration of the piston thrust damper with millimeter-size particles. We then investigated various system parameters to find their effects on the damping. Finally, began an investigation of the particle damping

mechanisms and the energy transfer and dissipation processes in our simulations. In the current year (2008-2009), we reported 1) the results from experiments on the passive particle-based thrust damping system, 2) the development of a semi-active particle-based damping system with tunable control 3) results from the particle dynamics-based simulation of the passive thrust damping system and 4) simulation based comparison of damping mechanism in a piston-type thrust damper vs. a box-type impact damper. All results are published in peer-reviewed journals and listed in the Publications section of this report.

Accomplishments

The focus of this research has been in three areas: mechanics of nanoparticles, experimental evaluation of piston-type and box-type dampers, and simulations based on computational particle dynamics. The results of these three areas are summarized next.

1. Mechanics of Nanoparticles

The mechanics of carbon nanoparticle chain aggregates (NCA, from the Friedlander group, UCLA) [1] were explored with the Ruoff group's home-built nanomanipulator inside the vacuum chamber of a dedicated FEI Nova 600 scanning electron microscope (SEM).

The carbon nanoparticle chains in an aggregate are strongly entangled with their neighbors and thus difficult to extract individually. Atomic force microscope (AFM) cantilevers with sharp tips were used to pull individual chains out from the aggregate. Eleven pulling attempts were performed and all the chains fractured before being completely pulled out. The measured breaking force for these carbon NCAs was around 41 nN.

To obtain well-defined stress/strain relations for isolated nanoparticle chains, two opposing AFM tips were used to stretch the two ends of a carbon nanoparticle chain (Figure 2a). Through nanomanipulation, the NCA was loaded in tension until fracture. The entire loading process was recorded with the movie-recording function of the SEM. From image analysis the stress-strain relationships of the NCAs under tension were obtained (Figure 2b). The measured tensile strengths range from 40 to 95 MPa.

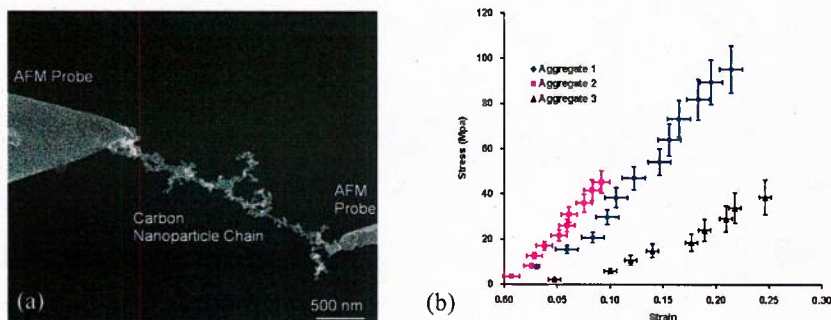


Figure 2. (a) An individual carbon nanoparticle chain being loaded in tension between two opposing AFM tips; (b) The stress-strain relationship of three carbon nanoparticle chains under tension.

The contact force between nanoparticles belonging to two different chains was also investigated. A short aggregate segment was attached to the AFM tip and the aggregate was brought into contact with another aggregate protruding from the NCA source. The AFM tip was then gradually pulled away from the source. The two aggregates separated at the original contact point. Three such tests were performed and the measured carbon aggregate contact forces were 4, 9 and 12 nN, respectively.

The van der Waals forces between two spherical particles can be calculated from the expression:

$$F_{vdw} = -\frac{H_a}{6} \cdot \frac{64R^6(h+2R)}{h^2(h+4R)^2(h^2+4Rh+4R^2)^2} \quad (1)$$

where H_a is the Hamaker constant ($\sim 2.53 \times 10^{-19}$ J for graphite and $\sim 7 \times 10^{-20}$ J for amorphous carbon), R is the radius of the primary particles (~ 15 nm), and h is the closest gap between the particle surfaces; For particles in contact, the gap (h) is assumed to be 2 and 6 Angstroms. The calculated van der Waals forces range from 1 to 8 nN for graphite and 0.2 to 2 nN for amorphous carbon, comparable with the experimental result.

2. Agglomeration and energy dissipation of nano-powders

We have studied the agglomeration of dry cohesive nano-powders using microscopy techniques and developed a mathematical model to represent the agglomerate structure and to calculate the energy dissipated during loading of the agglomerates.

Under the influence of the inter-particle adhesion, fine particles of the powders cluster together to form simple agglomerates. The simple agglomerates adhere together to form larger, complex agglomerates, which in turn, may adhere together and form a hierarchical structure (Fig. 3a-b). It is shown that contrary to diffusion-limited colloid aggregation, the simple agglomerates consisting of alumina or titanium dioxide particles are not mass fractals. The core structure of the simple agglomerates is described as a non-ordered homogeneous structure with a constant volume fraction (Fig. 3c), while the outer part (shell) can be considered as a rough surface that may have quite extended protuberances (Fig. 3b).

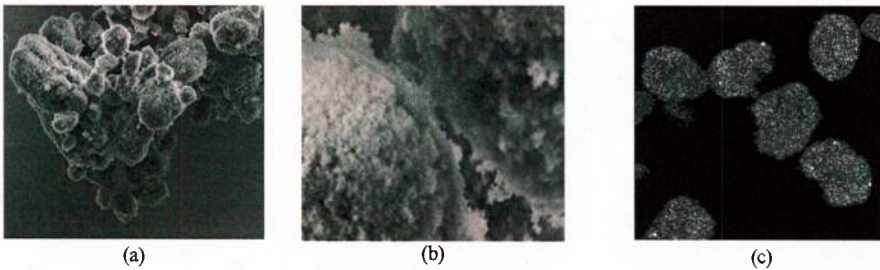


Fig. 3. (a) An SEM image showing a complex hierarchical structure of Al_2O_3 nanoparticle agglomerates. (b) Close-up of the interface from the alumina agglomerates, which are similar to those shown in (a). (c) An image of a cross section of several nano-particle agglomerates. The image is taken using a confocal microscope with 488 nm (blue laser). The bright spots on the image refer to a smaller cluster of particles and the dark areas refer to voids. It can be observed that the particles are organized in a uniform distribution within the agglomerates.

We hypothesized that energy could be dissipated in a nanoparticles system by fracturing the nanoparticles agglomerates. It is shown that the total energy dissipated during relative motion between simple agglomerates depends on the amount of the primary cycles - “jump into contact - pull off” between cohesive particles. The dissipated energy is equal to the number density of particle contacts in the fracture plane multiplied by the energy, w , dissipated in a single primary cycle. If we have two-level agglomerates then the total energy of dissipation U_{total} is

$$U_{total} = N^1 N_{cycles}^0 w \quad (2)$$

where N_{cycles}^0 is the average number of primary cycles during relative motion of two simple agglomerates and N^1 is the average number of simple agglomerates that were in contact during loading of the powder.

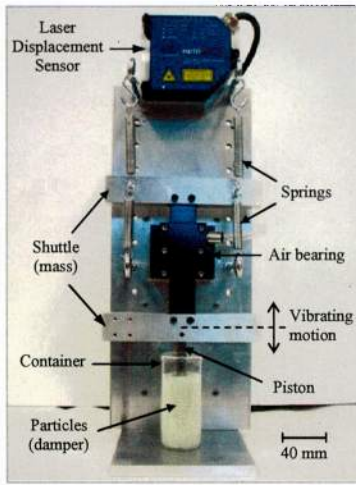
Since nano/micro particle agglomerates dissipate energy during the primary cycle “jump into contact - pull off” of contact between cohesive particles, they can be used as novel damping media. It is important to note that if the damper particles are repulsive or their contact properties are very close to particles described by the DMT model, then practically no energy is dissipated during the particle motion. On the other hand, if their contact properties are very close to those of the particles described by the JKR model, then cohesive forces may be too strong and the particles will stick together creating lumps (aggregates of high generation of the particles hierarchy) that cannot be crushed during damping. Hence, the dampers will not perform effectively. The best powders for dampers should have both quite large values of energy dissipated during a primary contact cycle and possibility to separate the particles from each other. They have to have also rather dense spatial structures of the aggregates that provide a large number of the primary adhesive contact cycles during the shift of the damper surfaces.

The three dimensional structure of agglomerates was experimentally studied using Confocal Microscopy (CFM), an optical imaging method. CFM provides information about the structure of nanoparticle agglomerates, which cannot be obtained using techniques such as Scanning Electron Microscopy (SEM). SEM was used to produce images that distinguish individual nanoparticles and their arrangements with high resolution and magnification (figure 3a-b). As a complementary method, CFM was used to non-destructively section agglomerates to reveal the assembly of particles inside individual cross-sections (fig. 3c). CFM was also used to create a three dimensional reconstruction of the agglomerates from its cross-sectioned images. Using a three-dimensional view, adhesion, interaction and arrangement of agglomerates can be better studied

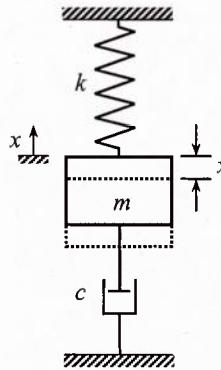
3. Experimental characterization of a passive thrust damping system

Experimental demonstration and performance characteristics of a particle-based thrust damping system for applications in extreme temperature applications have been presented. The damping behavior of dry and uncharged particles of silica, glass and steel has shown that damping is temperature independent, repeatable over consecutive tests, and effective even at low excitation levels where particle-based impact damping fails. The displacement decay is non-linear and therefore the damping behavior cannot be described by either a viscous or a frictional damping model.

A free vibrating mass-spring-damper system was built to experimentally characterize the particle-produced damping. The experimental setup of the system is shown in Fig. 4a and its equivalent model is illustrated in Fig. 4b. This system has the form of a thrust damper in which a piston vibrates vertically in a damping medium. The free vibration damping is characterized by measuring its displacement decay.



(a)



(b)

Figure 4. (a) Experimental setup designed to measure thrust damping, and (b) its equivalent system model in which k is the stiffness, m the mass, c the damping coefficient, and x the displacement of the mass from its equilibrium position.

Four extension springs are connected in parallel and attached to the shuttle to produce an undamped system of stiffness $k_n = 1985 \text{ N/m}$. A particle bed consisting of the damping media is held in a glass container. A cylindrical steel rod is used as the thrust piston with its top end attached to the bottom of the shuttle and the bottom end immersed into the particle bed. The sum of the weights of the shuttle and the piston is $m = 0.7 \text{ kg}$. The drag force exerted by the particle bed on the vibrating piston produces damping. In absence of the damping medium, the system is referred to as undamped. Nevertheless, the system still has inherent damping caused by factors such as internal friction and air resistance. A laser displacement sensor with displacement resolution of $1 \mu\text{m}$ and measurement frequency of 2500 Hz is used to measure the oscillations of the shuttle as a function of time t .

In this study, particles ranging from nanoscale to macroscale were used as the damping media, e.g. silica with average diameter $d = 15 \pm 5 \text{ nm}$, glass with $d = 50 \pm 10 \mu\text{m}$ and $d = 1, 2, 3 \pm 0.1 \text{ mm}$, as well as steel particles with $d = 1, 2 \pm 0.1 \text{ mm}$. The images of some sample particles are shown in Fig. 2 and their physical properties are presented in Table 1. Particles were selected based on their shape, size and material properties. Glass and steel were selected because they are

widely used, well characterized and strong enough to endure repeated loadings. With their melting points greater than 1400°C , these particles can also sustain high temperatures. Particles were chosen to be smooth and spherical in order to ensure consistent particle packing and flow behavior.

The experiments described in this paper were all conducted using the following procedure. A reproducible particle bed was created by pouring the particles into a cylindrical glass container of inner diameter D_c and filling it to a column height of H . The particles were then stirred to create uniform random packing. The top of the particle bed is considered as a free surface, as no constraints were applied there. The steel piston of diameter D_p was immersed into the particle bed to a depth of L from the free surface and given an initial downward or upward displacement A_0 to provide initial potential energy to the system. The piston was then released and set into free vibration which was recorded by the laser. The ambient relative humidity during the experiments was $24 \pm 3\%$. Unless mentioned otherwise, the standard parameters used for experiments are as follows: $H = 70\text{ mm}$, $L = 35\text{ mm}$, $D_c = 54.6\text{ mm}$, $D_p = 9.5\text{ mm}$, and $A_0 = -10\text{ mm}$.

Table 1: Physical properties of silica, glass and steel particles used in the experiments

Material	Silica	Glass	Steel
Size scale (diameter d)	Nano (15 nm)	Micro (50 μm), Macro (1, 2, and 3 mm)	Macro (1 and 2 mm)
Density ρ [kg/m^3]	2500	250, 1550	7800
Young's modulus E [GPa]	94	63	193

The variables t_i^α are used to denote the discrete moments when $x(t)$ reaches its valley value ($\alpha=1$) and peak value ($\alpha=2$) during the i -th cycle for all $i \geq 1$. The system vibrates with a constant period, $\Delta t_i^\alpha = t_i^\alpha - t_{i-1}^\alpha$ and the frequency is obtained from $f = 1/\Delta t_i^\alpha = \sqrt{k/m}/(2\pi)$. Each cycle is comprised of a pair of up-stroke and down-stroke motions. Given the initial displacement as shown in Fig. 4, a motion from $x(t_i^1)$ to $x(t_i^2)$ is called *up-stroke* and a motion from $x(t_i^2)$ to $x(t_{i+1}^1)$ is *down-stroke*.

In general, damping models are classified into two categories: viscous and frictional. If the displacement $x(t_i^\alpha)$ demonstrates an exponential decay and the damped frequency f_d is less than the undamped frequency f_n , the damping is considered as viscous. In contrast, if $x(t_i^\alpha)$ demonstrates a linear decay and $f_d = f_n$, the damping is frictional. However, damping in the present system is non-linear and therefore cannot be simply described by either a viscous or a frictional model. Instead, the principle of energy conservation is used to describe the experimental data. Accordingly, the total energy $E(t)$ of a system is equal to the sum of potential energy $U(t)$ and kinetic energy $K(t)$, i.e., $E(t) = U(t) + K(t)$. At the moments when

$t = t_i^\alpha$, the velocity is zero, and therefore the kinetic energy is zero. As a result, the energy in the system is $E(t_i^\alpha) = \frac{1}{2}kx^2(t_i^\alpha)$. The energy lost within one cycle is obtained by $W(t_i^\alpha) = E(t_i^\alpha) - E(t_{i+1}^\alpha)$, and the ratio of energy lost per cycle to the initial system energy is $W(t_i^\alpha)/E(t_i^\alpha)$. The damping efficiency per cycle is given by the specific damping capacity $\Psi(t_i^\alpha)$. It is the ratio of the energy lost within one cycle to the energy at the start of the cycle as follows

$$\Psi(t_i^\alpha) = \frac{W(t_i^\alpha)}{E(t_i^\alpha)} = \frac{x^2(t_i^\alpha) - x^2(t_{i+1}^\alpha)}{x^2(t_i^\alpha)}. \quad (3)$$

A decay time constant τ is used as a measure of the overall damping effectiveness. We define the value of τ as the time required for the system to reach $1/e$ of the initial energy $E(t_i^\alpha)$.

Damping with 1 mm glass particles. A damping experiment under free vibrations was conducted using 1 mm diameter glass particles. The vibrations were measured and the energy decay computed. The displacements $x(t)$ of the piston for a particle-damped and an undamped response are shown in Fig. 5. The displacement decay of the undamped system is negligible. The frequency for the damped system is $f_d = 8.82$ Hz and for the undamped system is $f_n = 8.47$ Hz., i.e., $f_d > f_n$ by 0.35 Hz or 4%. This frequency behavior is an unusual characteristic for a damping system. Generally $f_d < f_n$ in a particle-based impact damping or a fluid-based viscous damping system, and $f_d = f_n$ in a frictional damping systems. The increase in frequency is caused by either an increase in the stiffness k of the system or a decrease in the mass m . Since the mass is constant at $m = 0.7$ kg, the stiffness of the damped system ($k_d = 2150$ N/m) is 165 N/m or 8% greater than that of the undamped system ($k_n = 1985$ N/m). This implies that the stiffness of individual particles and the piston's motion in the particle bed can increase the damped frequency by increasing the overall stiffness of the system.

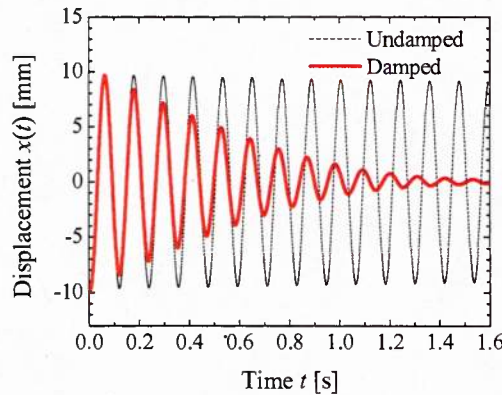


Figure 5. Displacement of the piston in a particle-damped (1mm glass) and an undamped system under free vibration.

The amplitudes $x(t_i^\alpha)$ at the minimum ($\alpha = 1$) and maximum ($\alpha = 2$) displacements are presented in Fig. 6a as the absolute value of the amplitude per stroke $|x(t_i^\alpha)|$. A stepwise trend in the amplitude decay was observed for consecutive up- and down-strokes of the piston. The change in amplitude was large during down-strokes but negligible during the up-strokes, which implies that damping did not occur equally throughout the duration of one cycle, but rather took place primarily during the downstroke of the piston. Such stepwise decay occurred due to the combination of two experimental conditions. The amplitude decay per cycle for the displacement $x(t_i^1)$ shows that the decay is rapid; the initial amplitude A_0 is reduced by 50 % in four cycles. In order to find the trend of the decay, $x(t_i^1)$ was fitted by an exponential and a linear function. As shown in Fig. 6a, neither function matched the decay trend. In addition, due to the unusual characteristic of the frequency, i.e., $f_d > f_n$, neither a viscous nor a frictional model could be used to describe the damping behavior. Therefore the use of a conventional damping factor to quantify the damping rate is not possible and damping appears to be non-linear. Instead, the critical decay time based on the energy conservation principle, described in section 3, is used to quantify the damping rate. The ratio of energy at the beginning of each cycle is compared to the initial energy of the system $E(t_i^\alpha)/E(t_1^\alpha)$ for $\alpha = 1$. The initial energy $E(t_1^1) = 107.5$ mJ for $|A_0| = 10$ mm and $k_d = 2150$ N/m. The critical decay time can be identified as $\tau = 0.36$ s, which is the time required to dissipate 63.3% of $E(t_1^1)$. The energy lost per cycle $W(t_i^\alpha)$ is reduced by an order of magnitude from 27.6 mJ to 2.6 mJ in the first eight cycles. In comparison, the undamped system loses a constant 0.7 mJ per cycle. Figure 7c plots the specific damping capacity $\Psi(t_i^\alpha)$, against the non-dimensional acceleration given by $\Gamma = 2\pi f_d^2 x(t_i^1)/g$, where g is the acceleration due to gravity.

Effect of particle size. The size of a particle determines the magnitude of its surface and body forces. The competition between these two forces affects the flow characteristics and thereby the damping performance. Damping experiments were conducted with particles of three different length scales, i.e. nanometer, micrometer and millimeter, in order to investigate the size effect. Particles of silica with $d = 15$ nm, and glass with $d = 50$ μ m, 1 mm and 3 mm were used in the experiments.

The amplitude decay for various particle sizes is presented in Fig. 6. A size effect can be clearly observed which shows that because of cohesive forces, damping is negligible with 15 nm particles but significantly greater with 1 mm and 3 mm particles. The difference in the damping rate between 1 mm and 3 mm particles is very small but that between 15 nm and 50 μ m particles is very large. In addition, damping rate decreases noticeably as the amplitude for the 3 mm particles drops below the particle size.

The weak damping performance of the 15 nm particles can be explained based on the following experimental observation. During the first down-stroke, as the piston entered the particle bed, the particles compacted together in the area between the piston and the container wall. As the piston moved out of the particle bed during the upstroke, the compacted particles retained their position and created a void about the size of the piston. The gravity force was unable to overcome the inter-particle cohesive force in order to reorganize the particles and fill the void. Therefore,

during the second down-stroke, the piston entered the void created previously and encountered no noticeable resistance. Although nanoparticles appear to be ineffective in this thrust-damping configuration, their ability to self-assemble into complex agglomerate structure provides them the potential to dissipate energy by fracturing their numerous inter-particle bonds.

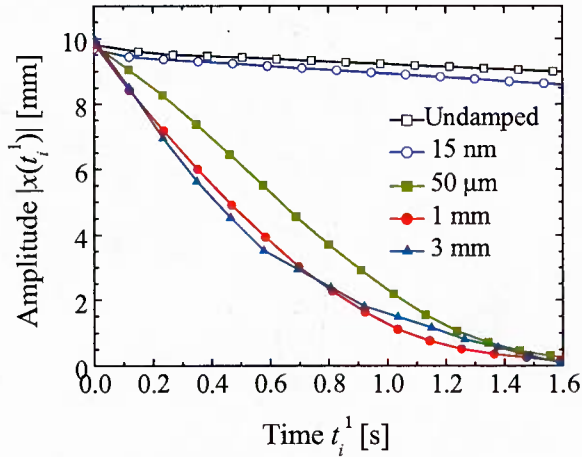


Figure 6. Amplitude decay per cycle showing the effect of particle size on damping performance.

Table 2 compares the critical decay time τ to Bo_g for the four particles tested, assuming $A_H = 10^{-20}$ J and $z = 0.2$ nm. The transition between cohesive and free-flowing particles is indicated by $Bo_g = 1$. For a particle such as 15 nm silica with $Bo_g \gg 1$, cohesive force is dominant and flow-ability is limited. Such particles demonstrate reduced effectiveness in thrust damping as indicated by the large decay time. On the other hand, when $Bo_g < 1$, as in the case of 3 mm particles, gravity force dominates, allowing for free-flow and reorganization of particles. Such particles enable very effective damping. In addition, the damping rate is more sensitive to variations in particle size at the nanometer and micrometer range than at the millimeter range. Furthermore, the bond number Bo_g can be a useful indicator in identifying the damping effectiveness of particles based on their cohesive flow properties.

Table 2. Critical decay time τ and the granular cohesive bond number Bo_g for particles of four sizes. The value of $Bo_g \gg 1$ implies that the particles are very cohesive. Such particles have low damping effectiveness as indicated by the large τ values.

Particle size (d)	Critical decay time τ [s]	Cohesive bond number Bo_g

Damped	Glass (3 mm)	0.31	0.15
	Glass (1 mm)	0.36	1.3
	Glass (50 μm)	0.52	520
	Silica (15 nm)	5.05	3.6×10^9
Undamped	N/A	6.80	N/A

Effect of particle mass. The mass of a particle can influence the particle flow behavior as well as the stress in the particle bed. Two experiments were conducted to investigate the effect of particle mass on the damping performance. Heavy and light weight spherical particles of equal diameters were selected for comparison. Particles with $d = 50 \mu\text{m}$ were used in the first experiment and with $d = 2 \text{ mm}$ in the second one. For the case with $d = 50 \mu\text{m}$, solid glass spheres with density $\rho = 1550 \text{ kg/m}^3$ were used as heavy particles and hollow glass spheres with $\rho = 250 \text{ kg/m}^3$ as light particles. For the case with $d = 2 \text{ mm}$, all the particles were spherical solids. Steel particles with $\rho = 7800 \text{ kg/m}^3$ were used as the heavy ones, while glass with $\rho = 1550 \text{ kg/m}^3$ as the lighter ones.

Figure 7 presents the energy decays for the two experiments and shows that the heavier particles dissipate energy faster than lighter ones for both particle sizes. In the case of $d = 50 \mu\text{m}$, $\tau = 0.52 \text{ s}$ for heavier particles and $\tau \sim 5.0 \text{ s}$ for the lighter ones. A ten fold increase in the damping rate is achieved by a six fold increase in particle weight. The lighter micro-particles have the same negligible damping rate, i.e. $\tau \sim 5.0 \text{ s}$, as that of the cohesive 15 nm silica particles (Table 2). In the case of $d = 2 \text{ mm}$, $\tau = 0.14 \text{ s}$ for the heavier particles and $\tau = 0.32 \text{ s}$ for the lighter ones. A five fold increase in the particle weight only doubled the damping rate.

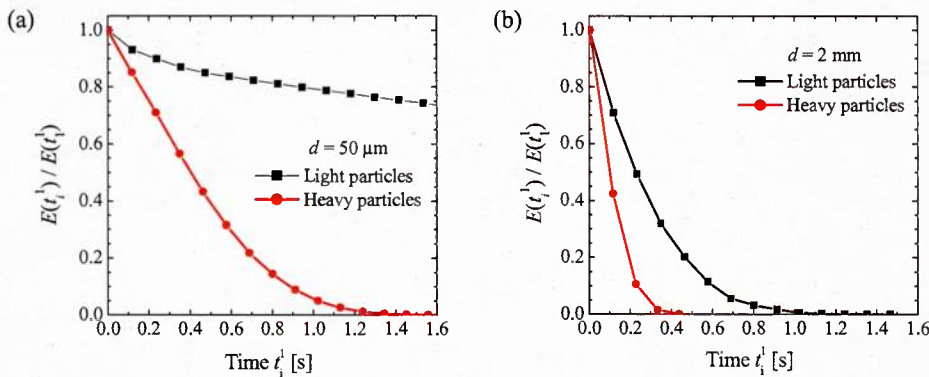


Figure 7. Comparison of energy decay between light and heavy particles of diameter $50 \mu\text{m}$ (a) and 2 mm (b).

Effect of Temperature. The primary advantage of a particle-damping medium is its ability to provide temperature independent damping. While the damping performance of a dry particle medium unlike a viscous fluid is said to be unaffected by large temperature variations [5, 6], apparently no experimental evidence has been reported in the literature. In this section, we experimentally evaluate the damping at temperatures ranging from 20°C to 130°C.

Glass particles of two different sizes, $d = 50 \mu\text{m}$ and $d = 1 \text{ mm}$, were used for evaluation. Experimental parameters were set to $A_0 = -5 \text{ mm}$ and $L = 25 \text{ mm}$. The particles were filled in a container, heated to 130°C and stirred to ensure uniform heating. Damping tests were performed periodically as the particles cooled from 130°C to 20°C at 40% relative humidity. The temperature T in the particle bed was continuously monitored. For each particle size, 47 damping tests were conducted over the entire temperature range. The damping performance for each test was evaluated in terms of the critical decay time τ . The results are shown in Fig. 10 as τ versus T for both particle sizes over the 110 degree temperature range.

The figure indicates that the damping performance is constant over the entire temperature range with negligible variations. The average value of τ for the 1 mm particles is 0.29 s with a standard deviation $\sigma = 0.0036$. For the 50 μm particles, τ is 0.31 s with $\sigma = 0.0062$. Such small values of σ indicate that the damping performance is temperature independent at both micrometer and millimeter scales. The temperature independence of a particle is limited by the melting point of its material. Therefore, materials with high melting point e.g., titanium dioxide (1870 °C) or tungsten carbide (2870 °C), can be used for extreme high temperature applications.

Figure 8 also illustrates the repeatability i.e. history independence, in this particle damping system. The fact that τ does not vary with consecutive tests suggests that the particle bed does not retain any memory from its previous tests that can influence its future tests. This history independent feature shows the potential for the particle damping system not just for one-time use applications, but also for multiple or continuous shock absorption.

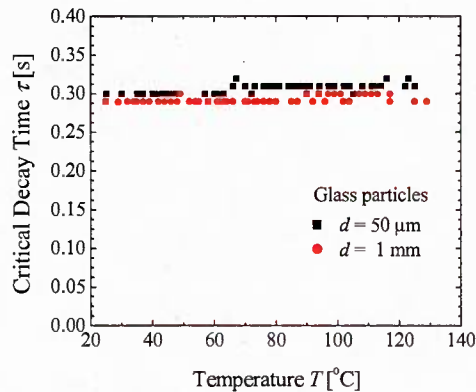


Figure 8. Effect of operating temperature on the damping performance of 50 μm and 1 mm diameter glass particles.

The size of the particle container, particularly its diameter, the sensitivity of damping to the start position of the piston based on three key parameters: (1) the immersion depth L of the piston's equilibrium position, (2) the sign of the amplitude A_0 with respect to the equilibrium ($A_0 = 0$), and (3) the magnitude $|A_0|$ of the amplitude were also investigated. The particle bed is shown to have an optimal value for its radius, below which piston jamming occurs and above which the size and mass of the device increase without providing additional damping. Damping rate is also sensitive to the piston's start position which is characterized by its immersion depth as well as the direction and magnitude of its initial amplitude. Displacement decay becomes faster with increasing piston immersion depth, greater damping is produced when the displacements start from above the equilibrium position i.e. $A_0 > 0$, and the damping rate is not affected by the variation in the initial amplitude when $A_0 < 0$.

4. Design of a semi-active particle-based thrust damping system

The damping efficiency is tunable by controlling the electric current supplied to generate a magnetic field. For the case in which a magnetic piston is used, the magnetization of both particles and pistons can improve the damping efficiency until the magnetization saturates. If both the particles and pistons are free of magnetic hysteresis, their demagnetization can reverse the damping system to its original un-magnetized status, i.e., the entire system is reversible during the process of magnetization and demagnetization. As a result, the damping rate is predictable, which ensures well-characterized tunability. In contrast, for the case with a non-magnetic piston, the damping system achieves the highest efficiency when particles are not magnetized, and the efficiency decreases with increasing magnetization. Under the tip of the non-magnetic piston, a void forms and its size increases as magnetization increases. It is the void that reduces the damping force and thus the efficiency.

Within a magnetic field, damping is proved to be independent of temperature for a certain temperature range. Specifically, damping with chrome steel particles is unaffected as the temperature varies between 20°C and 140°C, although the magnetization of the particles decreases by less than 20%. Furthermore, the magnetization of a single chrome steel particle is found unchanged when the temperature spans from -268°C to 0°C, which predicts that the damping performance would not be affected by temperature variation within this range.

5. Simulation of the particle-based thrust damping system

We used particle dynamics simulations to model the damping performance of piston-based particle dampers. The simulation results were compared and validated with experimental results which demonstrated that particle dynamics simulation can be used as a powerful tool to investigate the damping performance of particle dampers. Our results show that high damping capacity can be achieved in piston-based particle dampers. In our simulations, the Hertz-based contact force model was used as the force law in the normal direction and Coulomb's laws of friction were used as the force law in the tangential direction. Glass and steel particles were used as the damping medium in our simulations.

In the simulations, we found that the damping performance is very sensitive to the friction coefficient of particles and high friction coefficient is favorable for damping. On the other hand, it seems that the damping performance is insensitive to the coefficient of restitution for inelastic collision in the normal direction. This result implies that the energy dissipation is mainly through the frictional contact of particles. The particle size effect was also investigated in our simulation. We have found that the damping performance is insensitive to the particle diameter at the millimeter scale. At nanometer scale, however, the damping performance is very poor because the strong adhesive force between nanoparticles hinders their flowability. The particle immersion depth in the particle bed is also very important for the damping performance.

When two solid spheres with radii of R_i and R_j are brought into contact during a collision, a slight overlap is formed between them. If the distance between the two sphere centers is d_{ij} , then the overlap distance in the normal direction is $\alpha = R_i + R_j - d_{ij}$. Thus, the two spheres are in contact if $\alpha > 0$. The slight overlap induces a repulsive force in the normal direction, and the force-displacement relation can be described by many force models from contact mechanics [18-20, 24-28]. The simplest model is a linear spring model with velocity-dependent damping (linear spring-dashpot model), which is widely used for the inelastic collision. In this model, the normal contact force, f_n , can be expressed as

$$f_n = k_n \alpha - \gamma_n v_n, \quad (4)$$

where k_n is the normal stiffness, γ_n is the viscoelastic damping coefficient, and $v_n (= \dot{\alpha})$ is the relative velocity of two spheres in the normal direction. Note the negative sign of the damping term indicates that the damping force is always in the opposite direction of the relative velocity and therefore, always causes energy dissipation. If the initial relative velocity in the normal direction before the collision is v_n^i and the final relative velocity after the collision is v_n^f , then the coefficient of restitution is $e_n = -v_n^f / v_n^i$. In the Hertz-based contact model, the normal contact force is simply the product of the right-hand side of Eq. (4) and $\sqrt{\alpha}$,

$$f_n = k_n \alpha^{3/2} - \gamma_n v_n \sqrt{\alpha}. \quad (5)$$

In this model, the normal stiffness k_n is related to the Young's modulus (E), radius (R), and Poisson ratio (ν) of both spheres $k_n = \frac{4}{3} E^* \sqrt{R^*}$, where the effective radius R^* and the effective Young's modulus E^* can be calculated with $1/R^* = 1/R_i + 1/R_j$ and $1/E^* = (1-\nu_i^2)/E_i + (1-\nu_j^2)/E_j$.

In the tangential direction, the relative motion at the contact point between two touching bodies can be either static or dynamic. When the relative tangential velocity is zero ($v_s = 0$), the two bodies are in static contact. When $v_s \neq 0$, sliding or slip occurs between them. According to Coulomb's laws of friction, the frictional force in the tangential direction is directly related to the normal force through the following relation:

$$\begin{aligned} f_s &\leq \mu_s f_n, \text{ for static friction } (v_s = 0) \\ f_s &= \mu_d f_n, \text{ for dynamic friction } (v_s \neq 0) \end{aligned}$$

where μ_s and μ_d are the static and dynamic friction coefficients, respectively. Equation (4) indicates that the frictional force under the static condition is less than the threshold value ($\mu_s f_n$) and the actual static frictional force is exactly as same as the external shear force. The static frictional force is equal to the product of the shear elastic stiffness k_s and the shear displacement s , $f_s = k_s s$. The shear displacement s is the total traveling distance in the tangential direction starting from the established time of a contact. The overall shear force is the minimum of the static and dynamic friction forces,

$$f_s = -\min(|k_s s|, |\mu_d f_n|) \cdot \text{sign}(s), \quad (6)$$

where $\text{sign}(s)$ indicates the direction of the shear displacement. For the history-dependent shear force model, the ratio of k_s / k_n should be carefully chosen in order to keep the tangential collision time (t_s) very close to the normal collision time (t_n), i.e., $t_s / t_n \approx 1$. An alternative is to use a history-independent model in which the shear force is modeled by a simple viscous friction force: $-\gamma_s v_s$ for the linear model and $-\gamma_s \sqrt{\alpha} v_s$ for the Hertz-based model, where γ_s is the shear damping term. So the shear force in the history-independent model for the Hertzian contact can be expressed as

$$f_s = -\min(\gamma_s \sqrt{\alpha} v_s, |\mu_d f_n|) \cdot \text{sign}(v_s). \quad (7)$$

A direct comparison between the simulation and experiment is shown in Fig. 10. The simulation and experiment are in very good agreement. We found that using different configurations the simulations still agree with the experiments very well. Using this powerful simulation technique, we can investigate the detailed particle damping behaviors and mechanisms that are difficult or impossible to obtain in experiment. In order to reduce the computational load, in this work, we also use a small system as a model system to investigate the damping problems.

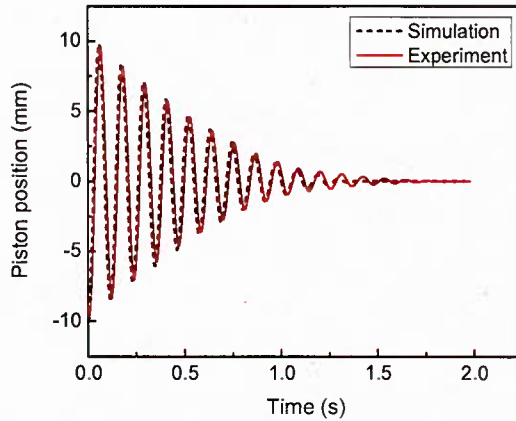


Fig. 5. A comparison of the piston damping curves between the simulation and experiment.

Simulation based understanding of the damping mechanisms

In particle damping, first energy is transferred from the vibrating structure to the particles. We found that energy transfer is mainly through collisions between the vibrating structure and the particles. We found that friction does not play an important role in energy transfer (but friction may be very important for energy dissipation, as noted in the next paragraph). The energy transfer in the box-type damper is more efficient than in the piston-type damper. We also found that the capacity for energy transfer affects the overall energy dissipation rate significantly. Consequently, the energy dissipation rate of the box-type damper is often faster than the piston-type damper in our simulations.

After energy is transferred to the particles, it is dissipated through friction and inelastic collisions between particles. For the steel particles studied in this work, friction dissipates more energy than the inelastic collisions. However, the relative importance between friction and collisions depends on the material properties of the particles and the excitation conditions. We also found that the overall particle damping performance depends on both energy transfer and the energy dissipation capacity. The two processes are not correlated, and thus, either one can become the limiting step. Depending on which one is the limiting step, the damping performance may or may not be sensitive to the friction coefficient. In addition to the particle-particle interactions, particle-wall interactions can also dissipate energy. Although the wall is very important for energy transfer, it does not play a significant role in energy dissipation.

Publications

1. Rong, W., Ding, W., Madler, L., Ruoff, R.S., Friedlander, S.K., Mechanical Properties of Nanoparticle Chain Aggregates by Combined AFM and SEM: Isolated Aggregates and Networks. *Nanoletters* Volume: 6 Issue: 12 Pages: 2646-2655 Published: DEC 13 2006.
2. X.-M. Bai, B. Shah, L.M. Keer, Q.J. Wang, R.Q. Snurr, "Particle dynamics simulations of a piston-based particle damper." *Powder Technology* **189**, 115-125 (2009).
3. B.L. Severson, L.M. Keer, J.M. Ottino, R.Q. Snurr, "Mechanical damping using adhesive micro or nano powders." *Powder Technology* **191**, 143-148 (2009).
4. B.M. Shah, D. Pillet, X.-M. Bai, L.M. Keer, Q.J. Wang, R.Q. Snurr, "Construction and characterization of a particle-based thrust damping system." *J. Sound and Vibration* **326**, 489-502 (2009).
- 5 X.-M. Bai, L.M. Keer, Q.J. Wang, R.Q. Snurr, "Investigation of particle damping mechanism via particle dynamics simulations." *Granular Matter*, (2009) 11:417-429.
6. B.M. Shah, J. Nudell, K. Kao, L.M. Keer, Q.J. Wang, "Semi-active particle-based thrust damping system controlled by magnetic fields." *J. Sound and Vibration*, (submitted).

Presentations at conferences

1. L. Keer et al., Investigation of Particle Damping Mechanism via Particle Dynamics Simulations and Experiments, *Leverhulme Trust Workshop on Adhesion*, St. Petersburg, Russia, June 2009.
2. B. Shah et al., Particle-Based Thrust Damping Technology for High Temperature Applications, *Presentation at GE Global Research Center*, Niskayuna, NY, Aug 19, 2008.
3. X.M. Bai, B. Shah, L. Keer, J. Wang, R. Snurr, Numerical Study of Particle Damping Mechanism in Piston Vibration System via Particle Dynamics Simulation, American Physical Society (APS) March Meeting, New Orleans, Louisiana, March 2008.
4. X.M. Bai, L. Keer, J. Wang, R. Snurr, Discrete Element Modeling of Close Box Oscillation with Granular Particles: Force Laws and Energy Dissipation (Poster), American Physical Society (APS) March Meeting, New Orleans, Louisiana, March 2008.

Formatted: Bullets and Numbering

Formatted: Bullets and Numbering

Discoveries, inventions, patents

L. Keer, B. Shah, Q. Wang and R. Snurr, Passive damping systems using dry multi-scale particles for temperature independent performance, September 2009. (Invention disclosure submitted)

Honors/Awards

1. Leon M. Keer received the Mayo D. Hersey Award from ASME. He was appointed Timoshenko Visiting Scholar in the Computational Division of the Mechanical Engineering Department at Stanford University.
2. Q. Jane Wang was elevated to Fellow, ASME 2009, and STLE 2007.
3. Randall Q. Snurr was appointed as Leibniz Professor at the University of Leipzig, Germany, for the summer 2009 semester.
4. Binoy M. Shah received a Student Intern/Co-op Contribution Award from General Electric Company and a Mentor Award from The Graduate School at Northwestern University.

Personnel

Faculty: Leon M. Keer, Randall Q. Snurr, Qian (Jane) Wang

Post Doc: Dr. Xianming Bai

Graduate Students: Binoy Shah (Ph.D. Candidate)

Undergraduate students: Kevin Kao and Jeremy Nudell